

# Molecular Mechanics Simulation of Buckling of Single-Walled Carbon Nanotubes

S.N. Korobeynikov<sup>1,a</sup>, V.V. Alyokhin<sup>1,b</sup>, and A.V. Babichev<sup>2,c</sup>

<sup>1</sup> Lavrentyev Institute of Hydrodynamics, Novosibirsk, Russia

<sup>2</sup> Sobolev Institute of Geology and Mineralogy, Novosibirsk, Russia

<sup>a</sup> s.n.korobeynikov@mail.ru, <sup>b</sup> alekhin@hydro.nsc.ru, <sup>c</sup> babichev@iggm@nsc.ru

**Keywords:** Molecular mechanics method, single-walled carbon nanotube, buckling.

**Abstract.** The molecular mechanics (MM) method is used to determine the critical buckling parameters and post-critical deformation modes of single-walled carbon nanotubes twisted at the edges. Computer simulation of the buckling and post-critical deformation of nanotubes is performed using two versions of the MM method: the standard MM method and a mixed method combining the molecular mechanics and molecular structural mechanics approaches (MM/MSM method). Computer simulation shows that the MM/MSM method gives acceptable critical twisting angles, buckling modes, and post-critical deformed configurations of nanotubes, comparable to the critical twisting angles, modes, and configurations obtained using the standard MM method.

## 1. Introduction

The use of carbon nanotubes has a significant place in modern nanotechnologies [1]. This is primarily due to their relatively low cost of manufacture and unique mechanical properties, namely, high rigidity and strength. However, single-walled carbon nanotubes (SWCNTs) can buckle and thus lose the desired performance even at relatively low compression and torsion loads. Therefore, the determination of the critical buckling parameters and the simulation of the post-critical deformation of nanotubes is an important area of nanomechanics.

Problems of nanotube deformation are solved using Newton's equations of particle motion in force fields. In this paper, by particles are meant carbon atoms of a nanotube which interact through short-range covalent forces and long-range non-covalent van der Waals (vdW) forces. In nanomechanics, Newton's equations are commonly solved using the molecular dynamics (MD) (cf., [2]) and molecular mechanics (MM) (cf., [3]) methods. In the present work, we employ the MM method since, in contrast to the MD method, it allows the use of nanotubes buckling criteria (cf, [3]) and a reliable determination of the critical parameters of nanotube deformation and buckling modes under the action of conservative external forces (cf., [4]).

The MM method, in turn, can be divided into the standard MM method (cf., [4,5]) and the molecular structural mechanics (MSM) method (cf., [6-9]). The standard MM method directly uses the potential interaction laws between atoms of a nanostructure, and in the MSM method, interatomic interactions are approximated by fictitious elastic trusses. In our previous studies of the use of the stability analysis of discrete elastic systems to study the buckling of nanotubes [4,10-12], we considered the following potential energies of interatomic interactions: the potential energy of covalent bond stretching, the potential energy of bond-angle variation, and the potential energy of non-covalent vdW forces between nanotube atoms. The potential energy of covalent bond stretching was determined using the Morse potential function, the potential energy of vdW forces was determined using the Lennard-Jones potential function, and the potential energy of bond-angle variation was modeled, following [6-9], through the use of the potential strain energy of strain of

fictitious elastic trusses. That is, in previous studies [4,10-12] we used a mixed molecular mechanics / molecular structural mechanics (MM/MSM) method which combines elements of the standard MM and the MSM techniques.

The purpose of the present study is to perform a comparative analysis of the solutions of buckling and post-buckling problems for twisted SWCNTs obtained by the standard MM method and the mixed MM/MSM method.

The results of this analysis are used to determine the range of applicability of the mixed MM/MSM method.

## 2. Interatomic energy of a SWCNT

We consider the covalent bond energy between carbon atoms of a nanotube, which is the sum of  $N$  bond-stretching energies, and  $L$  bond-angle bending energies, and the energy of  $J$  vdW bonds between the nanotube atoms. The potential energy of the internal forces of the nanotube is equal to the sum of the potential energies of all its elements, i.e.,

$$V = \sum_{n=1}^N V_b(r_n) + \sum_{l=1}^L V_\theta(\theta_l - \theta_0^l) + \sum_{j=1}^J V_{vdW}(r_j), \quad (1)$$

where  $V_b(r_n)$  ( $1 \leq n \leq N$ ) is the potential energy of the  $n$ -th bond stretching of carbon atoms ( $r_n$  is the interatomic distance in this bond),  $V_\theta(\theta_l - \theta_0^l)$  ( $1 \leq l \leq L$ ) is the energy of change of the  $l$ -th angle  $\theta^l$  between adjacent covalent bonds ( $\theta_0^l$  is the initial value of this angle),  $V_{vdW}(r_j)$  ( $1 \leq j \leq J$ ) is the vdW energy of the  $j$ -th non-covalent bond between atoms separated by a distance  $r_j$ . We assume that covalent bonds between atoms in nanotubes are constant (only the interaction force of these bonds can change), i.e., the integer numbers  $N$  and  $L$  are constant, and the number of the considered non-covalent bonds  $J$  can change during the motion of the nanotube. For the potential energy of an atomic bond element, we use the Morse potential function

$$V_b(r) \equiv D[e^{-2\alpha(r-r_e)} - 2e^{-\alpha(r-r_e)}], \quad (2)$$

where  $D$  is the depth of the potential hole,  $r_e$  is the interatomic distance that corresponds to the minimum potential energy of bond stretching, and  $\alpha$  is a specified parameter that determines the form of the potential.

For the potential energy of the vdW forces, we use the Lennard-Jones potential function [1,2,13]

$$V_{vdW}(r) \equiv \begin{cases} 4\varepsilon \left[ \left( \frac{\sigma}{r} \right)^{12} - \left( \frac{\sigma}{r} \right)^6 \right] & \text{if } 0 < r \leq r_{\text{cof}}, \\ 0 & \text{if } r > r_{\text{cof}}, \end{cases} \quad (3)$$

where  $\sigma, \varepsilon$  are prescribed constants.

In the standard MM method, the bond-angle bending energy is modeled using the potential function [14,15]

$$V_\theta(\theta - \theta_0) \equiv \frac{1}{2} k_\theta (\theta - \theta_0)^2 [1 + k_s (\theta - \theta_0)^4], \quad (4)$$

where  $k_\theta$  and  $k_s$  are given constants.

In the mixed MM/MSM method (combining the standard MM method and the MSM method), the bond-angle bending energy is approximated using the potential strain energy of some truss element [6-9]

$$V_i(r) \equiv \frac{1}{2} r_0 k e^2(r), \quad e \equiv \frac{r - r_0}{r_0}, \quad (5)$$

where  $k$  is the rigidity modulus of the truss element ( $k \equiv EA$ , where  $E$  is Young's modulus of the material of the truss element, and  $A$  is the cross-sectional area of this element),  $r_0$  is the initial length of the truss element. It can be shown [6-9] that, for a small change in the angle  $\theta$  ( $\theta - \theta_0 \ll 1$  rad) and for  $k_s = 0$ , the bond-angle bending energy (4) is approximated by the strain energy of the truss element (5) with the rigidity modulus

$$k = \frac{12k_\theta}{r_0}. \quad (6)$$

### 3. Molecular mechanics equations for a nanotube

The vector equation of motion for a nanotube with specified initial conditions is written as follows [5]:

$$\mathbf{M}\ddot{\mathbf{U}} + \mathbf{F}(\mathbf{U}) = \mathbf{R}, \quad \mathbf{U}(0) = \mathbf{U}_0, \quad \dot{\mathbf{U}}(0) = \mathbf{V}_0 \quad (\mathbf{F}, \mathbf{U}, \mathbf{R}, \mathbf{U}_0, \mathbf{V}_0 \in R^{NEQ}, \quad \mathbf{M} \in R^{NEQ} \times R^{NEQ}). \quad (7)$$

Here  $\mathbf{U}$ ,  $\mathbf{F}$ , and  $\mathbf{R}$  are the displacement and internal and external force vectors of the nanotube, respectively;  $\mathbf{U}_0$  and  $\mathbf{V}_0$  are the specified initial displacement and velocity vectors, respectively;  $\mathbf{M} > 0$  is the diagonal mass matrix with the masses of the nanotube atoms on the diagonal; the dot above a quantity denotes the derivative of this quantity with respect to time;  $NEQ$  is the total number of independent degrees of freedom of the nanostructure, i.e., the number of scalar equations of motion in system (7).

Neglecting inertial forces, from (7) we obtain the equilibrium equations for the nanotube

$$\mathbf{F}(\mathbf{U}) = \mathbf{R}. \quad (8)$$

The equations of quasi-static motion for the nanotube are obtained by differentiating the left- and right-hand sides of Eq. (8) with respect to a certain monotonically increasing deformation parameter, which, for simplicity, we still call the time  $t$ . Using the equality  $\dot{\mathbf{F}} = (\partial \mathbf{F} / \partial \mathbf{U}) \dot{\mathbf{U}}$ , we obtain the Cauchy problem

$$\mathbf{K}\dot{\mathbf{U}} = \dot{\mathbf{R}}, \quad \mathbf{U}(0) = \mathbf{U}_0. \quad (9)$$

Here we introduced the symmetric tangential stiffness matrix (Hessian matrix) of the ensemble of nanotube atoms

$$\mathbf{K} \equiv \frac{\partial \mathbf{F}}{\partial \mathbf{U}} = \frac{\partial^2 V}{\partial \mathbf{U} \partial \mathbf{U}}. \quad (10)$$

The vector  $\mathbf{F}$  and the matrix  $\mathbf{K}$  are obtained from the internal force vectors  $\mathbf{F}^e$  and the tangential stiffness matrices  $\mathbf{K}^e$  ( $1 \leq e \leq M$ ,  $M \equiv N + L + J$ ) of all the nanotube elements by the assembly operation [5]

$$\mathbf{F}(\mathbf{U}) = \mathbf{A} \sum_{m=1}^M \mathbf{F}^m(\mathbf{U}^m), \quad \mathbf{K}(\mathbf{U}) = \mathbf{A} \sum_{m=1}^M \mathbf{K}^m(\mathbf{U}^m). \quad (11)$$

Here  $\mathbf{U}^m$  is the displacement vector of the  $m$ -th element of the nanotube.

In this work, we deal with nanotube elements that have two-body (an element consists of atoms 'A' and 'B') and three-body (an element consists of atoms 'A', 'B', and 'C') potentials (Fig. 1).



Fig. 1. Elements used to model SWCNTs: (a) two-body potential element; (b) three-body potential element.

The displacement vector of an element with a two-body potential has the form

$$\mathbf{U}^e \equiv [u_1^A, u_2^A, u_3^A, u_1^B, u_2^B, u_3^B]^T \equiv [U_1, U_2, \dots, U_6]^T, \quad (12)$$

and the displacement vector of an element with a three-body potential has the form

$$\mathbf{U}^e \equiv [u_1^A, u_2^A, u_3^A, u_1^B, u_2^B, u_3^B, u_1^C, u_2^C, u_3^C]^T \equiv [U_1, U_2, \dots, U_9]^T. \quad (13)$$

Hereinafter,  $u_i^A$ ,  $u_i^B$ , and  $u_i^C$  are the  $i$ -th ( $i=1,2,3$ ) displacement components of atoms 'A', 'B', and 'C', respectively, in the atomic triad; the superscript ' $T$ ' denotes the transposition operation. The internal force vector  $\mathbf{F}^e$  and the symmetric tangential stiffness matrices  $\mathbf{K}^e$  of an element are expressed in terms of the potential energy of the element  $V^e$  as follows:

$$\mathbf{F}^e = \frac{\partial V^e}{\partial \mathbf{U}^e}, \quad \mathbf{K}^e \equiv \frac{\partial \mathbf{F}^e}{\partial \mathbf{U}^e} = \frac{\partial^2 V^e(\mathbf{U}^e)}{\partial \mathbf{U}^e \partial \mathbf{U}^e}. \quad (14)$$

Two-body potential elements (Fig. 1,a) include atomic pairs with covalent bond-stretching energies (having the potential energy  $V_b$ ), atomic pairs formed by vdW interactions (having the potential

energy  $V_{vdW}$ ), and atomic pairs of truss elements (having the potential energy  $V_i$ ). Expressions for the internal force vector  $\mathbf{F}^e$  and the tangential stiffness matrices  $\mathbf{K}^e$  of a two-body potential element (Fig. 1,a) were derived in [3,5]. We give these expressions following [5]:

$$\mathbf{F}^e = f\mathbf{B}^T, \quad \mathbf{K}^e = c\mathbf{B}^T \mathbf{B} + \frac{f}{r}(\mathbf{P} - \mathbf{B}^T \mathbf{B}), \quad (15)$$

where

$$f = \frac{\partial V^e(r)}{\partial r}, \quad c \equiv \frac{\partial f(r)}{\partial r} = \frac{\partial^2 V(r)}{\partial r^2}. \quad (16)$$

In (15) we introduced the row vector  $\mathbf{B}$  of size 6 and the matrix  $\mathbf{P}$  of size  $6 \times 6$ :

$$\mathbf{B} \equiv [-e_1, -e_2, -e_3, e_1, e_2, e_3], \quad \mathbf{P} \equiv \begin{bmatrix} \mathbf{I} & -\mathbf{I} \\ -\mathbf{I} & \mathbf{I} \end{bmatrix}, \quad \mathbf{I} \equiv \begin{bmatrix} 1 & 0 & 0 \\ 0 & 1 & 0 \\ 0 & 0 & 1 \end{bmatrix}. \quad (17)$$

Here  $e_k \equiv r_k / r$  ( $k=1,2,3$ ) are components of the unit length vector  $\mathbf{e} = [e_1, e_2, e_3]^T$ :

$$\mathbf{e} \equiv \mathbf{r} / r, \quad \mathbf{r} \equiv \mathbf{x}_B - \mathbf{x}_A, \quad r = \sqrt{\mathbf{r}^T \mathbf{r}}, \quad (18)$$

where  $\mathbf{x}_A$  and  $\mathbf{x}_B$  are the position vectors of atoms 'A' and 'B'.

In our case, the three-body potential elements are elements that take into account the energy  $V_\theta$  of change of the angle  $\theta$  between adjacent bonds (Fig. 1,b). The internal force vector  $\mathbf{F}^e$  and the tangential stiffness matrices  $\mathbf{K}^e$  of a three-body potential element were obtained in [3], and they can be represented as

$$\mathbf{F}^e = a\mathbf{M}^T, \quad \mathbf{K}^e = b\mathbf{M}^T \mathbf{M} + a\mathbf{N}, \quad (19)$$

where

$$a \equiv -\frac{k_\theta(\theta - \theta_0)}{\sqrt{1 - q^2}} [1 + 3k_s(\theta - \theta_0)^4], \quad q \equiv \mathbf{n}_1^T \mathbf{n}_2, \quad (20)$$

$$b \equiv \frac{k_\theta}{1 - q^2} \left\{ 1 + 15k_s(\theta - \theta_0)^4 - \frac{\theta - \theta_0}{\sqrt{1 - q^2}} [1 + 3k_s(\theta - \theta_0)^4] q \right\}.$$

Here  $\mathbf{n}_1$  and  $\mathbf{n}_2$  are unit length vectors (see Fig. 1,b):

$$\mathbf{n}_1 \equiv \frac{\mathbf{r}_{BA}}{r_{BA}}, \quad \mathbf{n}_2 \equiv \frac{\mathbf{r}_{BC}}{r_{BC}}, \quad \mathbf{r}_{BA} \equiv \mathbf{r}_A - \mathbf{r}_B, \quad \mathbf{r}_{BC} \equiv \mathbf{r}_C - \mathbf{r}_B, \quad r_{BA} \equiv |\mathbf{r}_{BA}|, \quad r_{BC} \equiv |\mathbf{r}_{BC}|. \quad (21)$$

In (19) we introduced the row vector of length 9

$$\mathbf{M} \equiv [\mathbf{M}_1, \mathbf{M}_2, \mathbf{M}_3], \quad (22)$$

where  $\mathbf{M}_1$ ,  $\mathbf{M}_2$ , and  $\mathbf{M}_3$  are row vectors of length 3

$$\mathbf{M}_1^T \equiv \frac{1}{r_{BA}} (\mathbf{n}_2 - q\mathbf{n}_1), \quad (23)$$

$$\mathbf{M}_2^T \equiv -\frac{1}{r_{BA}} (\mathbf{n}_2 - q\mathbf{n}_1) - \frac{1}{r_{BC}} (\mathbf{n}_1 - q\mathbf{n}_2) = -(\mathbf{M}_1^T + \mathbf{M}_3^T),$$

$$\mathbf{M}_3^T \equiv \frac{1}{r_{BC}} (\mathbf{n}_1 - q\mathbf{n}_2),$$

and the symmetric matrix  $\mathbf{N}$  of size  $9 \times 9$

$$\mathbf{N} = \begin{bmatrix} \mathbf{N}_{11} & \mathbf{N}_{12} & \mathbf{N}_{13} \\ \mathbf{N}_{21} & \mathbf{N}_{22} & \mathbf{N}_{23} \\ \mathbf{N}_{31} & \mathbf{N}_{32} & \mathbf{N}_{33} \end{bmatrix}, \quad (24)$$

where  $\mathbf{N}_{ij}$  ( $i, j = 1, 2, 3$ ) are matrices of size  $3 \times 3$ :

$$\mathbf{N}_{11} = \frac{1}{r_{BA}^2} [3q\mathbf{n}_1\mathbf{n}_1^T - \mathbf{n}_2\mathbf{n}_1^T - \mathbf{n}_1\mathbf{n}_2^T - q\mathbf{I}], \quad (25)$$

$$\mathbf{N}_{12} = \frac{1}{r_{BA}} \left[ \left( \frac{1}{r_{BC}} - \frac{3q}{r_{BA}} \right) \mathbf{n}_1\mathbf{n}_1^T + \frac{1}{r_{BC}} \mathbf{n}_2\mathbf{n}_2^T + \frac{1}{r_{BA}} \mathbf{n}_2\mathbf{n}_1^T + \left( \frac{1}{r_{BA}} - \frac{q}{r_{BC}} \right) \mathbf{n}_1\mathbf{n}_2^T + \left( \frac{q}{r_{BA}} - \frac{1}{r_{BC}} \right) \mathbf{I} \right],$$

$$\mathbf{N}_{13} = \frac{1}{r_{BA}r_{BC}} [\mathbf{I} - \mathbf{n}_1\mathbf{n}_1^T - \mathbf{n}_2\mathbf{n}_2^T + q\mathbf{n}_1\mathbf{n}_2^T],$$

$$\mathbf{N}_{22} = \left( \frac{2}{r_{BA}r_{BC}} - \frac{q}{r_{BA}^2} - \frac{q}{r_{BC}^2} \right) \mathbf{I} + \left( \frac{3q}{r_{BA}^2} - \frac{2}{r_{BA}r_{BC}} \right) \mathbf{n}_1\mathbf{n}_1^T + \left( \frac{3q}{r_{BC}^2} - \frac{2}{r_{BA}r_{BC}} \right) \mathbf{n}_2\mathbf{n}_2^T + \left( \frac{q}{r_{BA}r_{BC}} - \frac{1}{r_{BA}^2} - \frac{1}{r_{BC}^2} \right) (\mathbf{n}_1\mathbf{n}_2^T + \mathbf{n}_2\mathbf{n}_1^T),$$

$$\mathbf{N}_{23} = \frac{1}{r_{BC}} \left[ \left( \frac{1}{r_{BA}} - \frac{3q}{r_{BC}} \right) \mathbf{n}_2\mathbf{n}_2^T + \frac{1}{r_{BA}} \mathbf{n}_1\mathbf{n}_1^T + \frac{1}{r_{BC}} \mathbf{n}_2\mathbf{n}_1^T + \left( \frac{1}{r_{BC}} - \frac{q}{r_{BA}} \right) \mathbf{n}_1\mathbf{n}_2^T + \left( \frac{q}{r_{BC}} - \frac{1}{r_{BA}} \right) \mathbf{I} \right],$$

$$\mathbf{N}_{33} = \frac{1}{r_{BC}^2} [3q\mathbf{n}_2\mathbf{n}_2^T - \mathbf{n}_2\mathbf{n}_1^T - \mathbf{n}_1\mathbf{n}_2^T - q\mathbf{I}],$$

$$\mathbf{N}_{21} = \mathbf{N}_{12}^T, \quad \mathbf{N}_{31} = \mathbf{N}_{13}^T, \quad \mathbf{N}_{32} = \mathbf{N}_{23}^T.$$

#### 4. Results of numerical simulation of deformation and buckling of twisted SWCNTs

The atomic bond, truss, bond-angle bending, and vdW interaction elements were implemented in the finite element library of the PIONER code [16]. Numerical solutions of the problems of deformation

and buckling of SWCNTs were obtained with the help of this code. The problems of quasi-static or dynamic nanotube deformations were solved by step-by-step integration of the MM equations of quasi-static or dynamic motion; in the latter case, we used the Newmark method [17]. In each integration step, the solution was refined using the iterative procedure of the Newton-Raphson method [17].

The constants of the potential functions (2)-(4) for SWCNTs have the following values [13-15]:

$$r_e = 0.142 \text{ nm}, \quad \alpha = 26.25 \text{ nm}^{-1}, \quad D = 0.603105 \text{ nN}\cdot\text{nm}, \quad k_\theta = 0.9 \text{ nN}\cdot\text{nm} / \text{rad}^2, \quad \sigma = 0.3412 \text{ nm},$$

$$r_{\text{cof}} = 0.45 \text{ nm}, \quad \varepsilon = 0.0003840 \text{ nN}\cdot\text{nm}, \quad m_a = 0.019927 \text{ nN}\cdot\text{ps}^2 / \text{nm},$$

where  $m_a$  is the mass of the carbon atom.

We solve the problems of deformation and buckling of a (10,10) armchair and a (10,0) zigzag SWCNTs and compare the obtained solutions with the solutions of these problems given in [4]. In the cited paper, we used the mixed MM/MSM method. In the present paper, we solve these problems using the standard MM method and then compare the obtained solutions with those presented in [4].

#### 4.1. Deformation and buckling of a (10,10) armchair SWCNT

Consider an armchair type SWCNT with chirality indices (10,10) of radius  $R = 0.6792 \text{ nm}$  and length  $L = 12.2919 \text{ nm}$ . The atoms at both edges of the SWCNT are constrained in the axial direction and move on circles of radius  $R$  with prescribed monotonically increasing twisting angle  $\varphi$  (Fig. 2,a). We find the first bifurcation points and their corresponding buckling modes by solving the quasi-static deformation problem (Fig. 3). In addition, we determine quasi-bifurcation points, their corresponding buckling modes, and post-critical deformation modes by solving dynamic problems of twisting of the nanotube at a rate  $\dot{\varphi} = 1.8 \text{ degr./ps}$ . To find the post-critical deformed configurations, we must subject nanostructure deformation to a small perturbation, possibly agreeing with the buckling mode(s) obtained at the (quasi-)bifurcation point on the integral curve of the solution. Henceforth, by solutions of unperturbed problems, we mean solutions obtained for the initial positions of the atoms in the nanostructure specified by using double precision arithmetic. Furthermore, for the initial configuration of the nanotube, the interatomic distances  $r_e$  are specified with a minimum accuracy of 13 significant digits. By solutions of problems with type #1 perturbations, we mean solutions obtained for the initial positions of atoms in the nanotube specified using up to the first five significant digits (i.e., simulating calculations using single precision arithmetic), and by solutions of problems with perturbations of type #2, we mean solutions obtained with specified additional compression forces applied to the atoms in the helix along the axial coordinate of the nanotube which have absolute values  $F = 10^{-3} \text{ nN}$  (these perturbations are fitted to the 3-half-wave buckling mode presented in Fig. 3,c). Since the first lower (quasi-)bifurcation points are close to each other (see Fig. 3,a,b), one can expect the development of post-critical deformation modes correlated with both the 3-half-wave buckling mode (see Fig. 3,c) and the 4-half-wave one (see Fig. 3,d). We observe two qualitatively different configuration modes for the initial post-critical deformation of the nanotube; that is, the configuration modes for the initial post-critical deformation obtained by solving the unperturbed problem and the problem with perturbations of types #1 correlate with the 4-half-wave buckling mode presented in Fig. 3,d (see the post-buckling configuration obtained by solving the unperturbed problem and presented in Fig. 4,a), and the configuration modes for the initial post-critical deformation obtained by solving the problem with perturbations of types #2 correlate with the 3-half-wave buckling mode presented in Fig. 3,c (see the post-buckling configuration obtained by solving the problem with perturbations of type #2 and presented in Fig. 4,b).

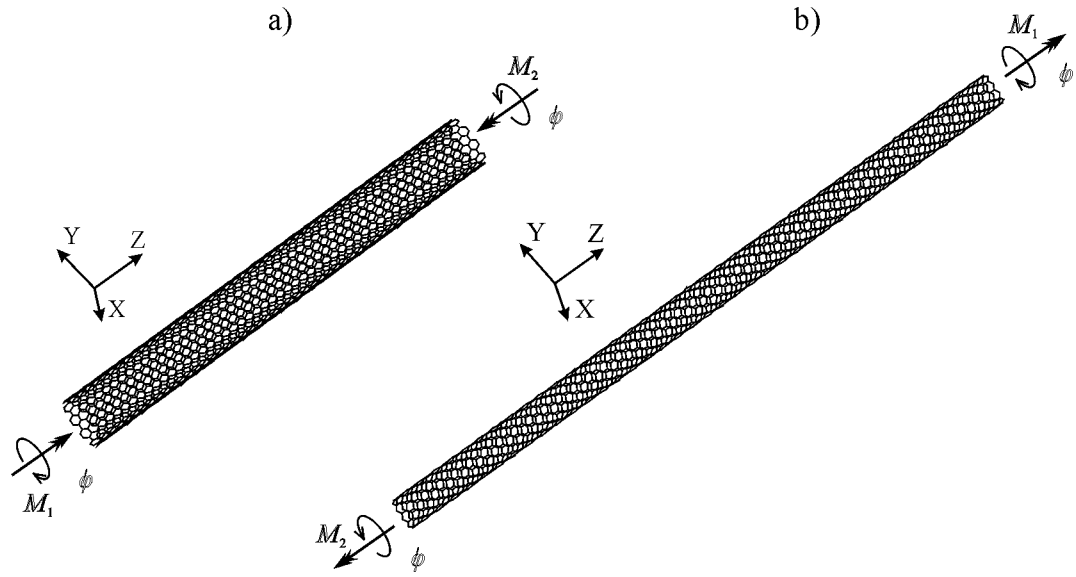


Fig. 2. Two twisted SWCNTs: a) a (10,10) armchair SWCNT; b) a (10,0) zigzag SWCNT.

The buckling modes and post-critical deformed configurations presented in Figs. 3 and 4 were obtained using the mixed MM/MSM method. The buckling modes and initial post-critical deformed configurations obtained using the standard MM method are close to the corresponding buckling modes and initial post-critical deformed configurations obtained using the mixed MM/MSM method. However, for large twisting angles ( $\varphi \geq 240^\circ$ ), the deformed configurations of the nanotube obtained using the standard MM method correspond to the fractured nanotube, and the deformed configurations of the nanotube obtained using the mixed MM/MSM method correspond to the unfractured nanotube up to a twisting angle  $\varphi = 360^\circ$  (see Fig. 5). From this and the fact that the potential energy of internal forces  $V$  obtained by solving the problem of nanotube twisting by the standard MM method is lower than the same energy obtained using the mixed MM/MSM method (see Fig. 3,a), it follows that the potential energy of the internal forces of truss elements obtained using the rigidity modulus in (6) gives overestimated rigidity compared with the energy for bond-angle bending elements.

#### 4.2. Deformation and buckling of a (10,0) zigzag SWCNT

Consider a zigzag type SWCNT with chirality indices of (10,0) of radius  $R = 0.3931$  nm and length  $L = 16.8980$  nm, subjected to twisting with some prescribed atom displacements at its edges (see Fig. 2,b). The atoms at the lower edge of the tube are constrained in the axial direction, and the atoms at the upper edge can move without constraints in this direction. We define unperturbed problems and problems with perturbations of type #1 as in Sect 4.1, and by solutions of problems with perturbations of types #2 and #3, we mean solutions obtained with specified additional compression forces applied to the atoms that have absolute values  $F = 10^{-3}$  nN (perturbations of types #2 and #3 are fitted to the buckling modes presented in Fig. 6,c and Fig. 6,d, respectively). We first solve the problem of quasi-static deformation and determine the first two bifurcation points in the fundamental solution (Fig. 6). We determine quasi-bifurcation points and their corresponding buckling modes and modes of post-critical deformation by solving the dynamic problem of nanotube twisting at a rate  $\dot{\varphi} = 3.6$  degr./ps (see Figs. 6,7). In contrast to the solution of the twisting problem for an armchair SWCNT presented in Sect. 4.1, from the solution of the problem presented in this

section, it follows that the zigzag SWCNT does not fracture up to a twisting angle  $\varphi = 360^\circ$  when using both the standard MM method and the mixed MM/MSM method (Fig. 8). As in Sect. 4.1, the potential energy of internal forces of truss elements gives overestimated rigidity compared with the energy of bond-angle bending elements.

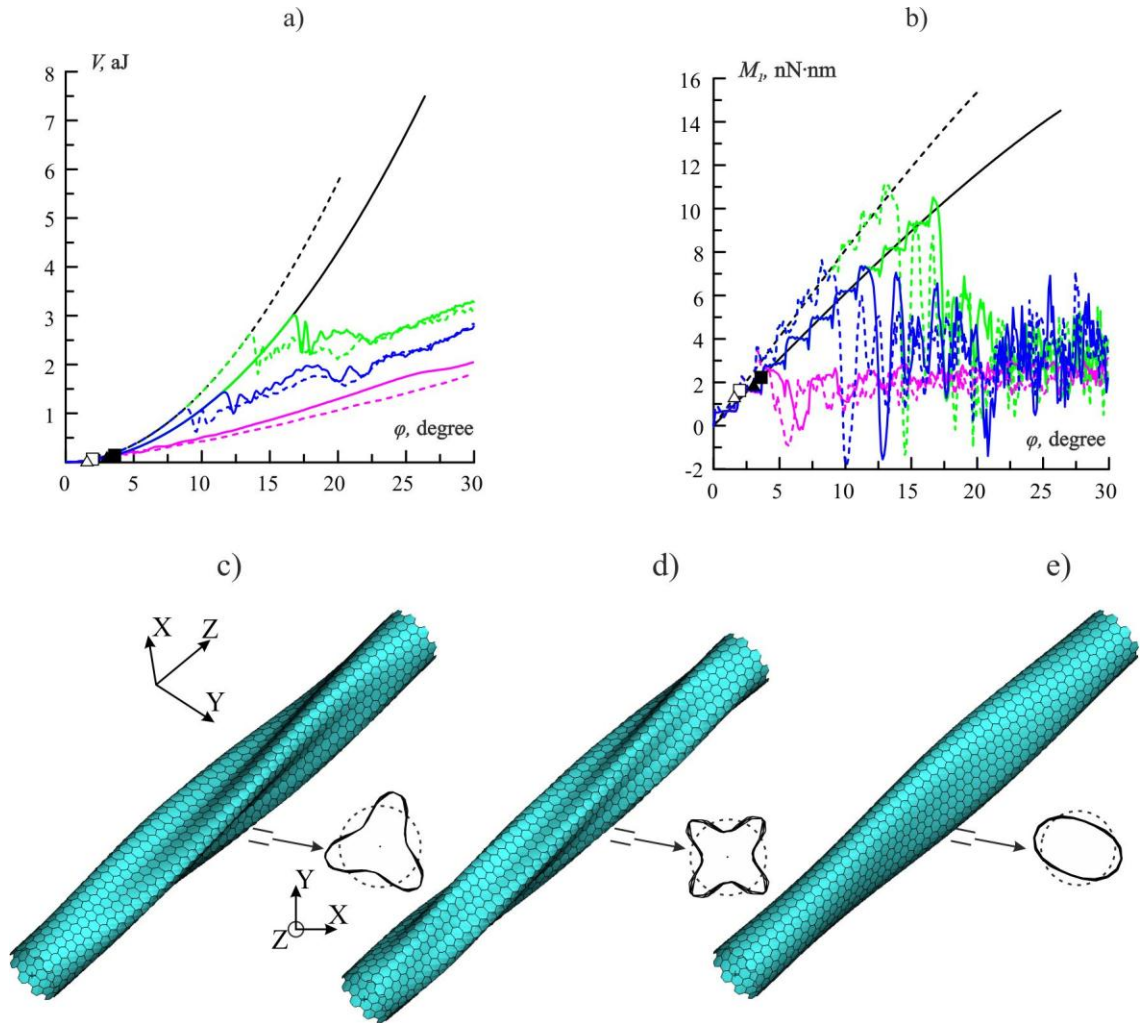


Fig. 3. Deformation and buckling of the twisted (10,10) armchair SWCNT: a), b) potential energy of internal forces  $V$  and torque  $M_1$  versus twisting angle  $\varphi$  (dashed curves correspond to the mixed MM/MSM method, and solid curves correspond to the standard MM method; black curves correspond to the quasi-static unperturbed problem, and color curves correspond to the dynamic problem for  $\dot{\varphi} = 1.8$  degr./ps: green curves correspond to the unperturbed problem, blue curves correspond to problem with perturbations of types #1, magenta curves correspond to the problem with perturbations of types #2); c), d) buckling modes at the bifurcation points marked by  $\Delta$ ,  $\blacktriangle$ , and  $\square$ ,  $\blacksquare$ , respectively, in a) and b) for the unperturbed problems (the points which are marked by  $\Delta$  and  $\square$ , they are obtained by the mixed MM/MSM method; the points which are marked by  $\blacktriangle$  and  $\blacksquare$ , they are obtained by the standard MM method); e) buckling mode at the (quasi-)bifurcation points (between the points marked by  $\blacktriangle$  and  $\blacksquare$ ) in the solution of the unperturbed problems by the standard MM method.

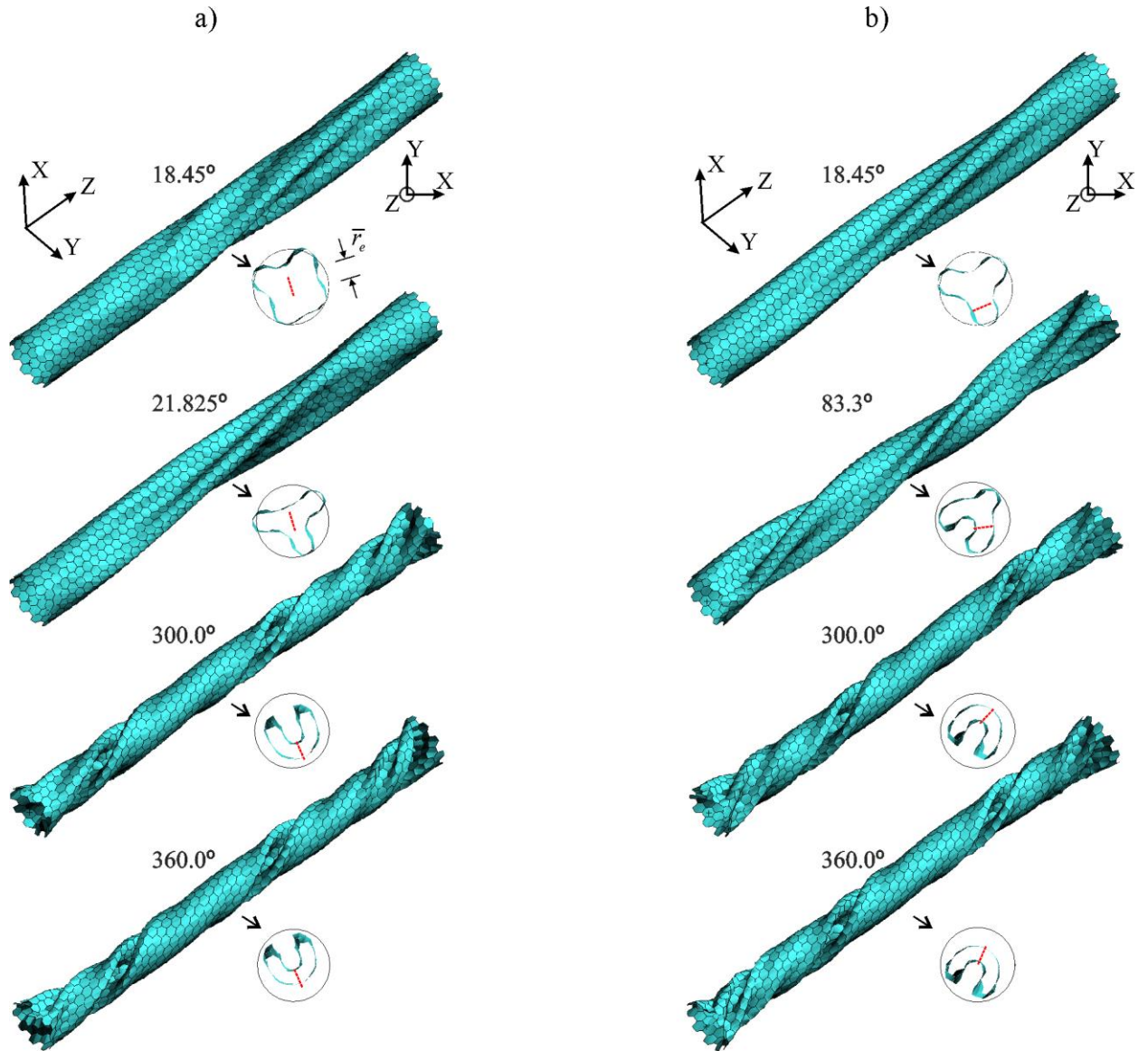


Fig. 4. Post-buckling configurations of the twisted (10,10) armchair SWCNT under dynamic deformation for  $\dot{\varphi} = 1.8$  degr./ps (values of the twisting angle  $\varphi$  are given near the deformed configurations) corresponding to the solutions of: a) the unperturbed problem; b) the problem with perturbations of type #2; the deformed configurations were obtained by the mixed MM/MSM method and correspond to the green and magenta dashed curves in Fig. 3,a,b.

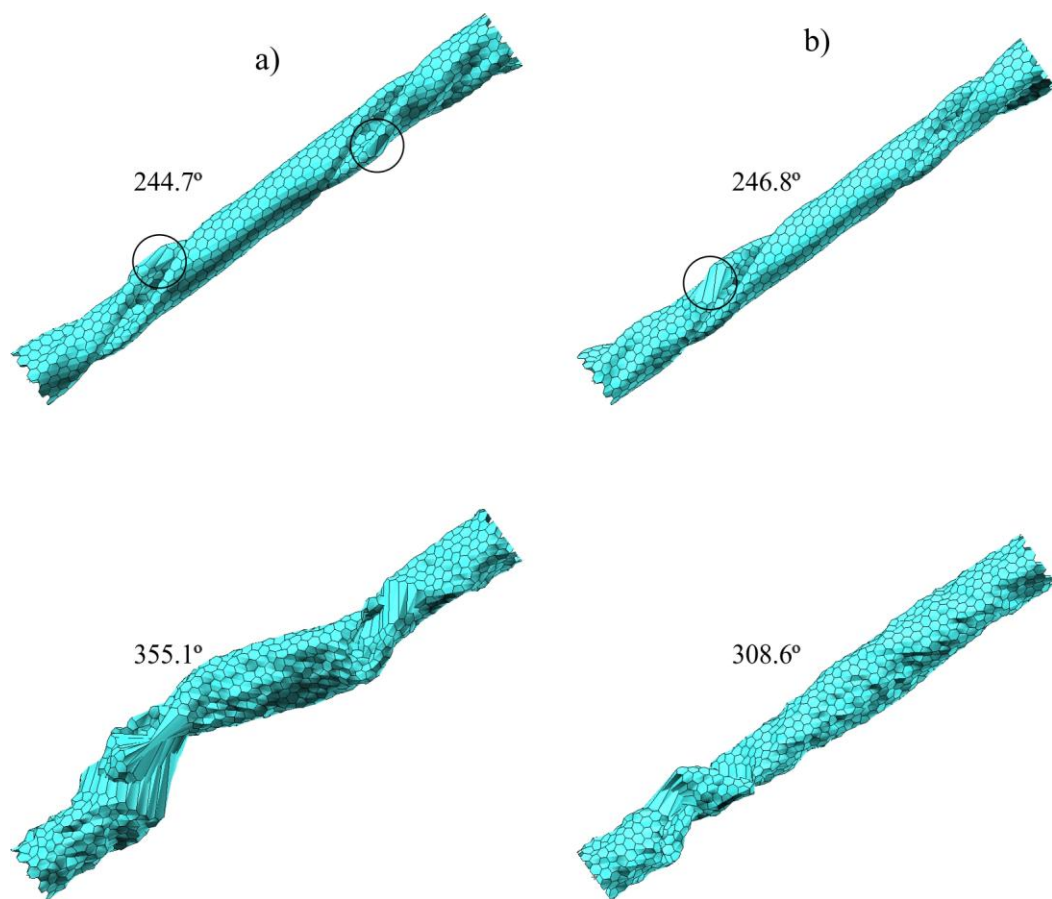


Fig. 5. Post-buckling configurations of the twisted (10,10) armchair SWCNT under dynamic deformation for  $\dot{\varphi} = 1.8$  degr./ps (values of the twisting angle  $\varphi$  are given near the deformed configurations) corresponding to the solutions of: a) the unperturbed problem; b) the problem with perturbations of type #2; the deformed configurations were obtained by the standard MM method, and correspond to the green and magenta solid curves in Fig. 3,a,b; circles show the regions of initiation of nanotube fracture.

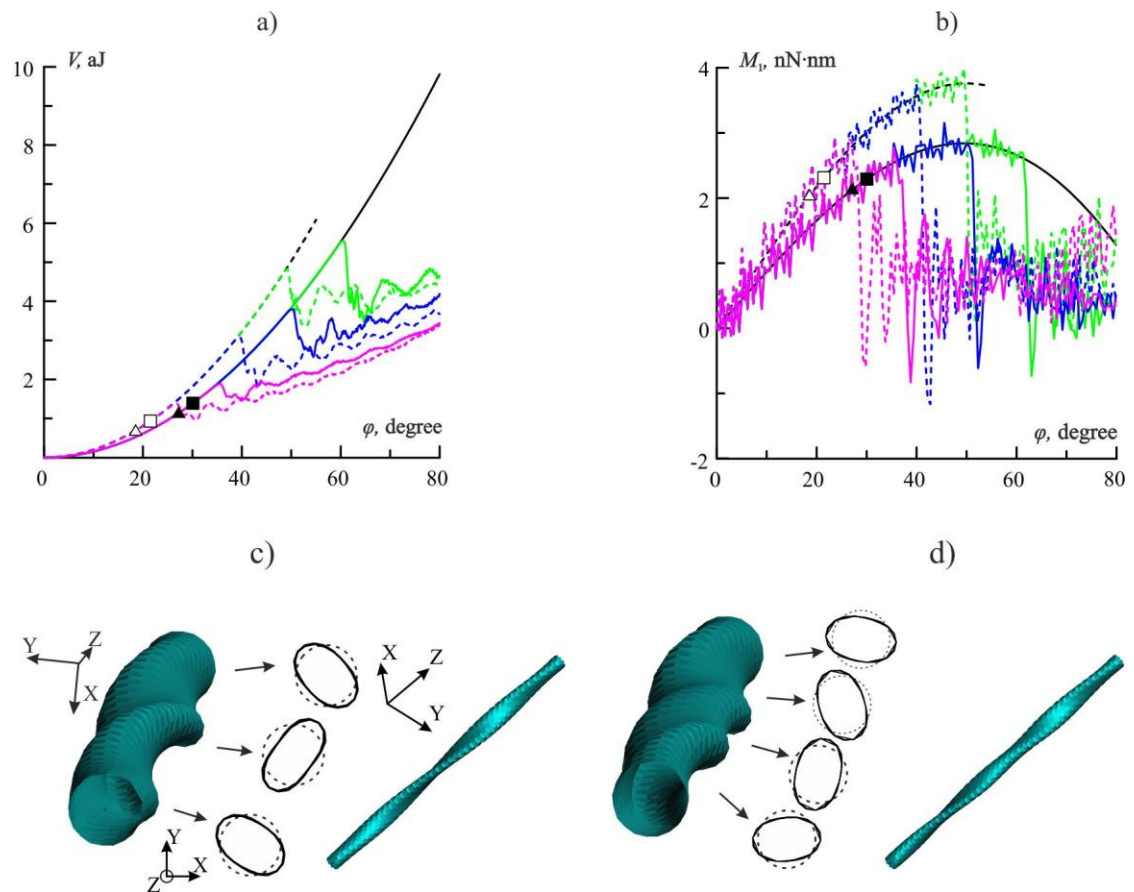


Fig. 6. Deformation and buckling of the twisted (10,0) zigzag SWCNT: a), b) potential energy of internal forces  $V$  and torque  $M_1$  versus twisting angle  $\phi$  (dashed curves correspond to the mixed MM/MSM method, and solid curves correspond to the standard MM method; black curves correspond to quasi-static unperturbed problems, and color curves to dynamic problems for  $\dot{\phi} = 3.6$  degr./ps: green curves correspond to the unperturbed problem, blue curves correspond to problems with perturbations of types #1, magenta curves correspond to problems with perturbations of types #2); c), d) buckling modes at the bifurcation points marked by  $\Delta$ ,  $\blacktriangle$ , and  $\square$ ,  $\blacksquare$ , respectively, in a) and b) for the unperturbed problems (the points which are marked by  $\Delta$  and  $\square$ , they are obtained by the mixed MM/MSM method; the points which are marked by  $\blacktriangle$  and  $\blacksquare$ , they are obtained by the standard MM method).

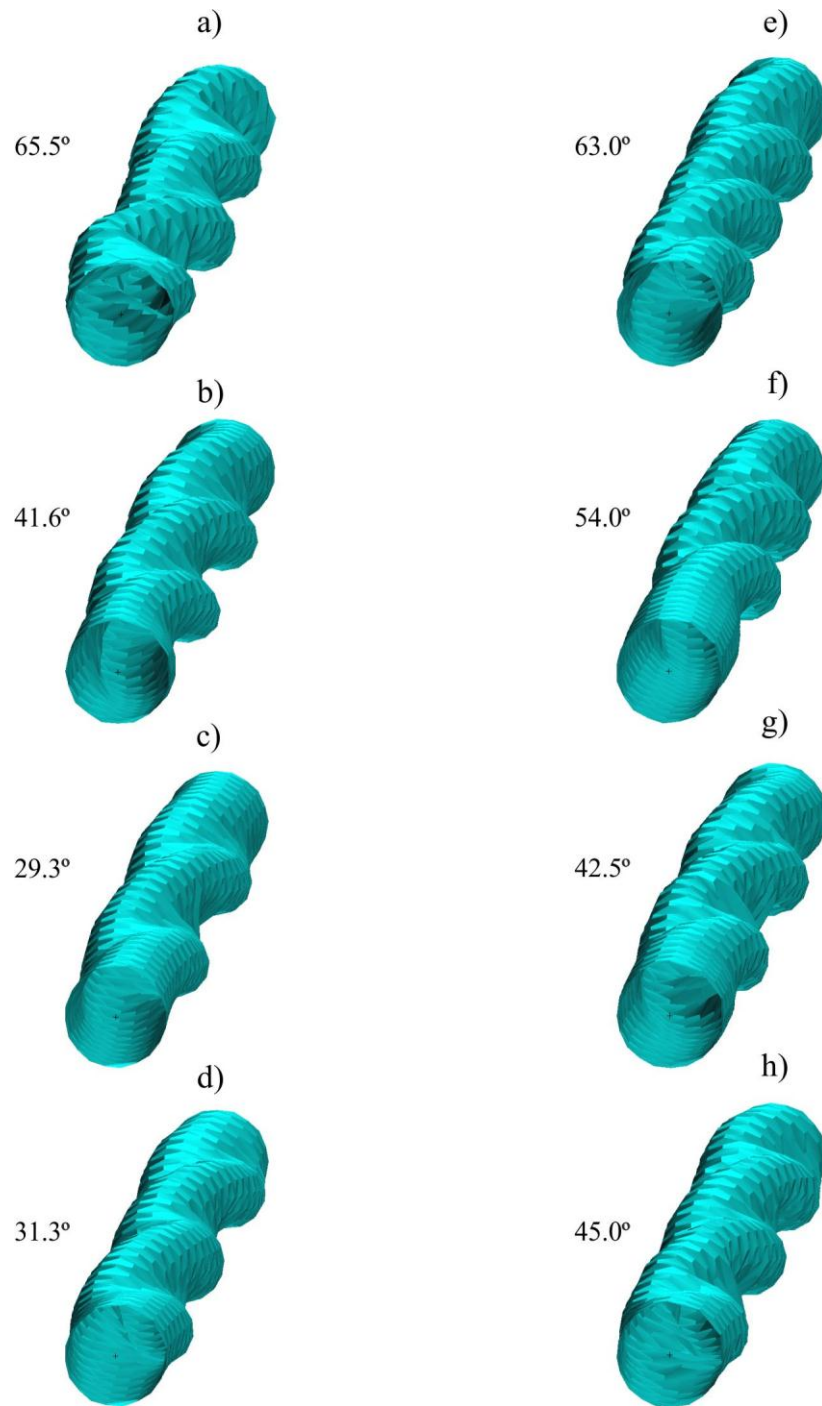


Fig. 7. Post-buckling configurations of the twisted (10,0) zigzag SWCNT under dynamic deformation for  $\dot{\varphi} = 3.6$  degr./ps (values of the twisting angle  $\varphi$  are given near the deformed configurations) obtained by the mixed MM/MSM method (see a), b), c), d)) and the standard MM method (see e), f), g), h)) and corresponding to the solutions of: a), e) the unperturbed problem; b), f) problems with perturbations of type #1; c), g) problems with perturbations of type #2; d), h) problems with perturbations of type #3.



Fig. 8. Post-buckling configurations of the twisted (10,0) zigzag SWCNT under dynamic deformation for  $\dot{\varphi} = 3.6$  degr./ps (values of the twisting angle  $\varphi$  are given near the deformed configurations) obtained in solutions of the unperturbed problems using: a) the mixed MM/MSM method; b) the standard MM method.

## Conclusions

The comparison of the solutions of the buckling problem for SWCNTs obtained by the standard MM method and the mixed MM/MSM method shows that the critical parameters, buckling modes, and post-critical deformation modes differ only slightly. However, the mixed MM/MSM method leads to a more rigid nanotube model compared with the standard MM method.

## Acknowledgements

The supports from the Russian Foundations for Basic Research (Grant No. 12-08-00707) and the program of fundamental research of Russian Acad. of Sci. (Project No. 25) are gratefully acknowledged.

## References

- [1] H. Rafii-Tabar: *Computational Physics of Carbon Nanotubes* (Cambridge Univ. Press, Cambridge 2008).
- [2] A.M. Krivtsov: *Deformation and Failure of Solids with Microstructure* (in Russian) (Fizmatlit, Moscow 2007).
- [3] J. Wackerfuss: *Int. J. Num. Meth. Engng.* Vol. 77 (2009), pp. 969-997.
- [4] S.N. Korobeynikov, V.V. Alyokhin, B.D. Annin, and A.V. Babichev: *Arch. Mech.* (2012), in press.
- [5] S.N. Korobeynikov: *Arch. Mech.* Vol. 57 (2005), pp. 457-475.
- [6] G.M. Odegard, T.S. Gates, L.M. Nicholson, and E. Wise: *Composites Science and Technology* Vol. 62 (2002), pp. 1869-1880.
- [7] T.S. Gates, G.M. Odegard, S.J.V. Frankland, and T.C. Clancy: *Composites Science and Technology* Vol. 65 (2005), pp. 2416-2434.
- [8] R.V. Goldstein and A.V. Chentsov: *Mech. Solids* Vol. 40 (2005), pp. 45-59.
- [9] R.V. Goldstein, A.V. Chentsov, R.M. Kadushnikov, and N.A. Shturkin: *Nanotechnologies in Russia* Vol. 3 (2008), pp. 112-121.
- [10] S.N. Korobeynikov and A.V. Babichev: in: *CD ICF Interquadrennial conference full papers*, edited by R.V. Goldstein, Institute for Problems in Mechanics, Moscow (2007).
- [11] B.D. Annin, S.N. Korobeynikov, and A.V. Babichev: *J. Appl. Ind. Math.* Vol. 3 (2009), pp. 318-333.
- [12] S.N. Korobeynikov, B.D. Annin, and A.V. Babichev: in: *CD Proceedings of the 18<sup>th</sup> European Conference on Fracture, Fracture of Materials and Structures from Micro to Macro Scale*, edited by D. Klingbeil *et al.*, Dresden (2010).
- [13] L.A. Girifalco, M. Hodak, and R.S. Lee: *Phys. Rev. B* Vol. 62 (2000), pp. 13104-13110.
- [14] T. Belytschko, S.P. Xiao, G.C. Schatz, and R.S. Ruoff: *Phys. Rev. B* Vol. 65 (2002), 235430.
- [15] J.M. Wernik and S.A. Meguid: *Acta Mech.* Vol. 212 (2010), pp. 167-179.
- [16] S.N. Korobeinikov, V.P. Agapov, M.I. Bondarenko, and A.N. Soldatkin: in: *Proc. Int. Conf. on Numerical Methods and Applications*, edited by B. Sendov *et al.*, Publ. House of the Bulgarian Acad. of Sci., Sofia (1989), pp. 228-233.
- [17] K.J. Bathe: *Finite Element Procedures* (Prentice Hall, Upper Saddle River, New Jersey 1996).